Heliyon 5 (2019) e02058

Contents lists available at ScienceDirect

Heliyon

journal homepage: www.heliyon.com

Comparative study of Cu–Zn coatings electrodeposited from sulphate and chloride baths

C. Oulmas [a,b], S. Mameri [a], D. Boughrara [a,*], A. Kadri [a], J. Delhalle [b], Z. Mekhalif [b], B. Benfedda [a]

[a] Laboratoire de Physique et Chimie des Matériaux, Université Mouloud MAMMERI de Tizi-Ouzou, BP 17 RP, Tizi-Ouzou, 15000, Algeria
[b] Laboratoire de Chimie et d'Electrochimie des Surfaces, Université de Namur, 61, Rue de Bruxelles, 5000, Namur, Belgium

ARTICLE INFO

Keywords:
Materials science
Electrochemistry
Sulphate
Chloride
Citrate
Cu–Zn alloy
Corrosion
Electrodeposition
Steel

ABSTRACT

In this work, the effect of the nature of the salt anion (chloride and sulphate) in the Cu–Zn citrate bath was investigated, using cyclic voltammetry (CV) and chronoamperometry (CA). Experimental electrodeposition parameters (switching potential and imposed potential) were varied in order to examine their influence on the deposits. The coating microstructures were observed by scanning electron microscope (SEM-EDS), the coating phases were characterized by X-ray diffraction (XRD) analysis and the surface composition was assessed by XPS. Higher current efficiency was obtained in chloride baths compared to sulphate baths and best deposits were obtained at -1.4 *V vs.*$(Ag/AgCl/KCl)$ compared to -1.2 and -1.5 *V vs.*$(Ag/AgCl/KCl)$. Corrosion test results in 0.5 M NaCl solution show that Cu–Zn deposit produced from chloride bath exhibited the highest corrosion resistance.

1. Introduction

Currently, zinc, copper and their alloys such as Zn–Cu [1], Zn–Sn [2], Zn–Ni [3], Zn–Mn [4], Ni–Sn [5], Cu–Sn [6], Cu–Ni [7] and Cu–Mn [8] are involved in a large range of industrial applications. They are used in protection against corrosion as well as in decorative, electrical and magnetic applications.

Among these alloys Cu–Zn, also called brass, electrodeposited for the first time in 1841 from a cyanide bath [9], is still of high interest in fundamental and applied research [10, 11, 12, 13, 14]. This is due to its low cost, environmental compatibility, mechanical strength, extreme hardness compared to pure metals coatings [10] and its beautiful colour that turns from red to golden yellow. These properties make it useful in many fields such as manufacture of precision instruments, electronic components and batteries.

Electrodeposition of Cu–Zn alloy is obtained using baths with complex composition, usually water as solvent, salts as metallic ion sources, acids to adjust the pH and additives such as complexing agents to reduce the potential difference between the two metals [15]. Cyanides have been conventionally used for Cu–Zn electrodeposition and have proven to be very efficient [14, 16, 17]. However, it is highly toxic and harmful to the environment. The elimination of cyanide waste and its decomposition during electrolysis are the major problems. Due to these disadvantages, alternative complex agents have been used, among them, pyrophosphate [17], triethanolamine [18], glycerol [14], EDTA [19], trilonate [20], pyrophosphate-oxalate [21], d-mannitol [22], sodium gluconate [23], tartrate [24], sorbitol [12] or glycine [1]. Citrates as complexing agent have been used for the electrodeposition of monometallic (Cu) [25], bimetallic (Cu–Zn) [13] and trimetallic (Zn–Co–Mo) coatings [26].

For instance, during the electrodeposition of FeCo, NiCo and CoNiFe alloys, Kim et al. [27] observed higher current efficiencies in chloride medium compared to sulphate bath. They have attributed these results to a catalytic effect of chloride which has also been demonstrated in the case of a copper deposit by some authors [28, 29, 30, 31].

In sulfate bath, copper deposition occurs according to the following consecutive reactions:

$$Cu^{2+} + e^- \rightleftarrows Cu^+ \text{ the rate determining step} \quad (1)$$

$$Cu^+ + e^- \rightleftharpoons Cu \quad (2)$$

The addition of Cl^- ions causes an acceleration in the reduction of copper ions by the formation of an adsorbed complex ($CuCl$) according to the reactions (3) and (4) that is parallel with the reactions (1) and (2).

$$Cu^{2+} + Cl^-_{ads} + e^- \rightleftharpoons CuCl_{ads} \quad (3)$$

* Corresponding author.
E-mail address: d_boughrara@yahoo.fr (D. Boughrara).

https://doi.org/10.1016/j.heliyon.2019.e02058
Received 17 October 2018; Received in revised form 12 June 2019; Accepted 5 July 2019

Table 1
Chemical composition in mol/L of Cu–Zn electrolysis baths.

Product\Bath		S1	S2	S3	S4	S5	S6
Sulphate	$ZnSO_4.7H_2O$	10^{-3}	–	10^{-3}	–	–	–
	$CuSO_4$	–	1.50×10^{-3}	1.50×10^{-3}	–	–	–
	Na_2SO_4	0.16	0.16	0.16	–	–	–
Chloride	$ZnCl_2$	–	–	–	10^{-3}	–	10^{-3}
	$CuCl_2.2H_2O$	–	–	–	–	1.50×10^{-3}	1.50×10^{-3}
	KCl	–	–	–	0.16	0.16	0.16
Additif	$Na_3C_6H_5O_7.2H_2O$	0.2	0.2	0.2	0.2	0.2	0.2
	$C_7H_4NNaSO_3.H_2O$	10^{-2}	10^{-2}	10^{-2}	10^{-2}	10^{-2}	10^{-2}
	H_3BO_3	0.40	0.40	0.40	0.40	0.40	0.40

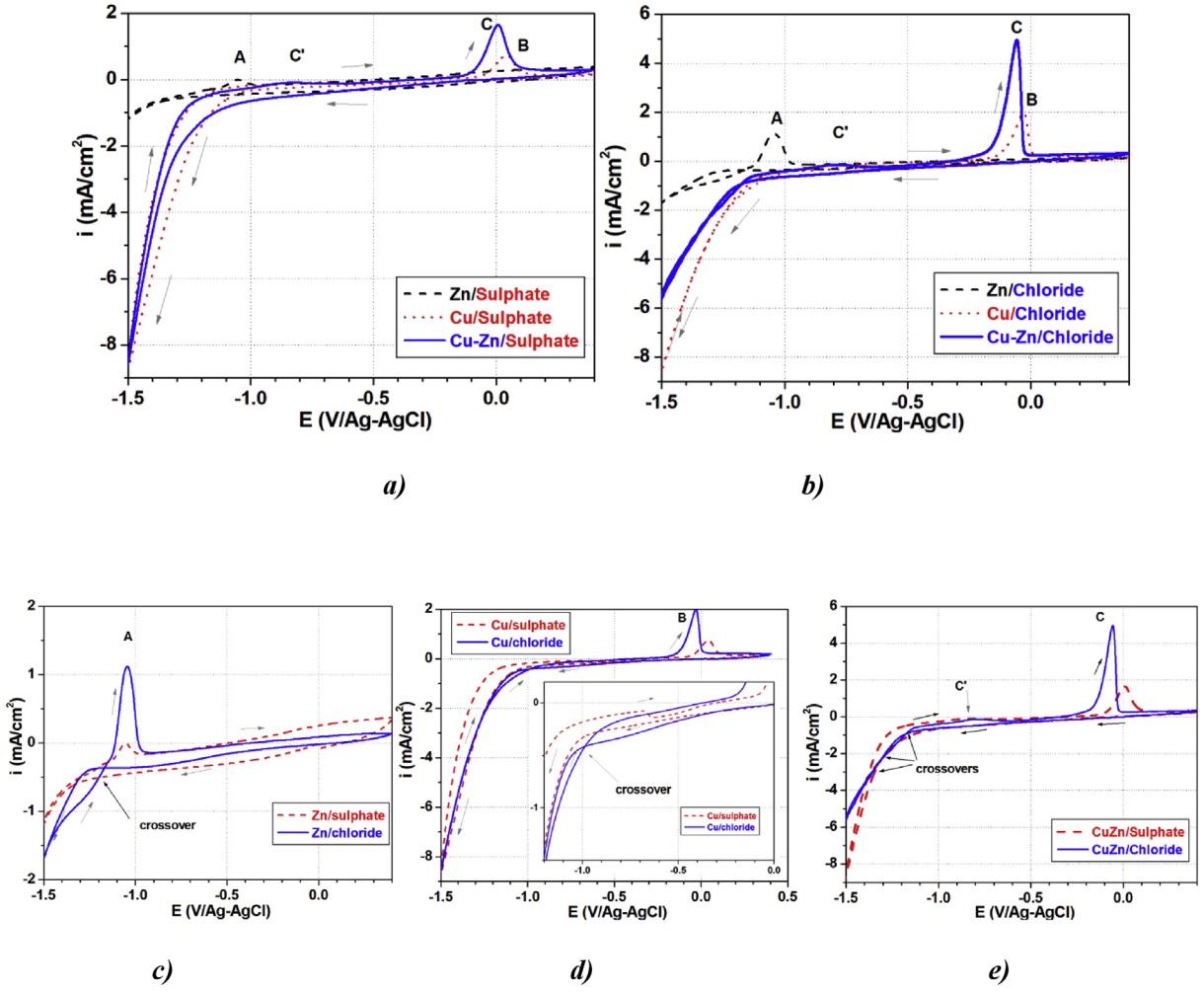

Fig. 1. Cyclic Voltammograms recorded on GC substrate at $S_R = 20$ mV s^{-1} and $\Omega = 250$ rpm a) in sulphate bath (S1, S2, S3) and b) in chloride bath (S4, S5, S6) and highlighting comparison of sulphate and chloride anions for c) Zn, d) Cu and e) Cu–Zn.

Table 2
Potential and current density values at the maximum of the anodic peaks from Fig. 1.

Bath	E_A (V)	i_A (mA.cm^{-2})	E_B (V)	i_B (mA.cm^{-2})	E_C (V)	i_C (mA.cm^{-2})	$E_{C'}$ (V)	$i_{C'}$ (mA.cm^{-2})
Sulphate	− 1.05	0.02	0.05	0.76	0	1.72	− 0.8	− 0.01
Chloride	− 1.05	1.14	− 0.03	2.05	− 0.06	5.02	− 0.8	0.01

$$CuCl_{ads} + e^- \rightleftharpoons Cu + Cl^- \quad (4)$$

The adsorbed Cl^- accelerate the overall reduction kinetics and acts as a dynamic template, which guides surface-step orientation and copper deposition. According to Horkans [32], the electrodeposition of NiFe in chloride electrolyte presents higher activity of metal ions and lower metal deposition potential compared to sulfate electrolytes. The presence of sulfate anions in the acidic gluconate baths of tin electrodeposition is found to inhibit cathodic process and to affect the morphology of tin deposits [33].

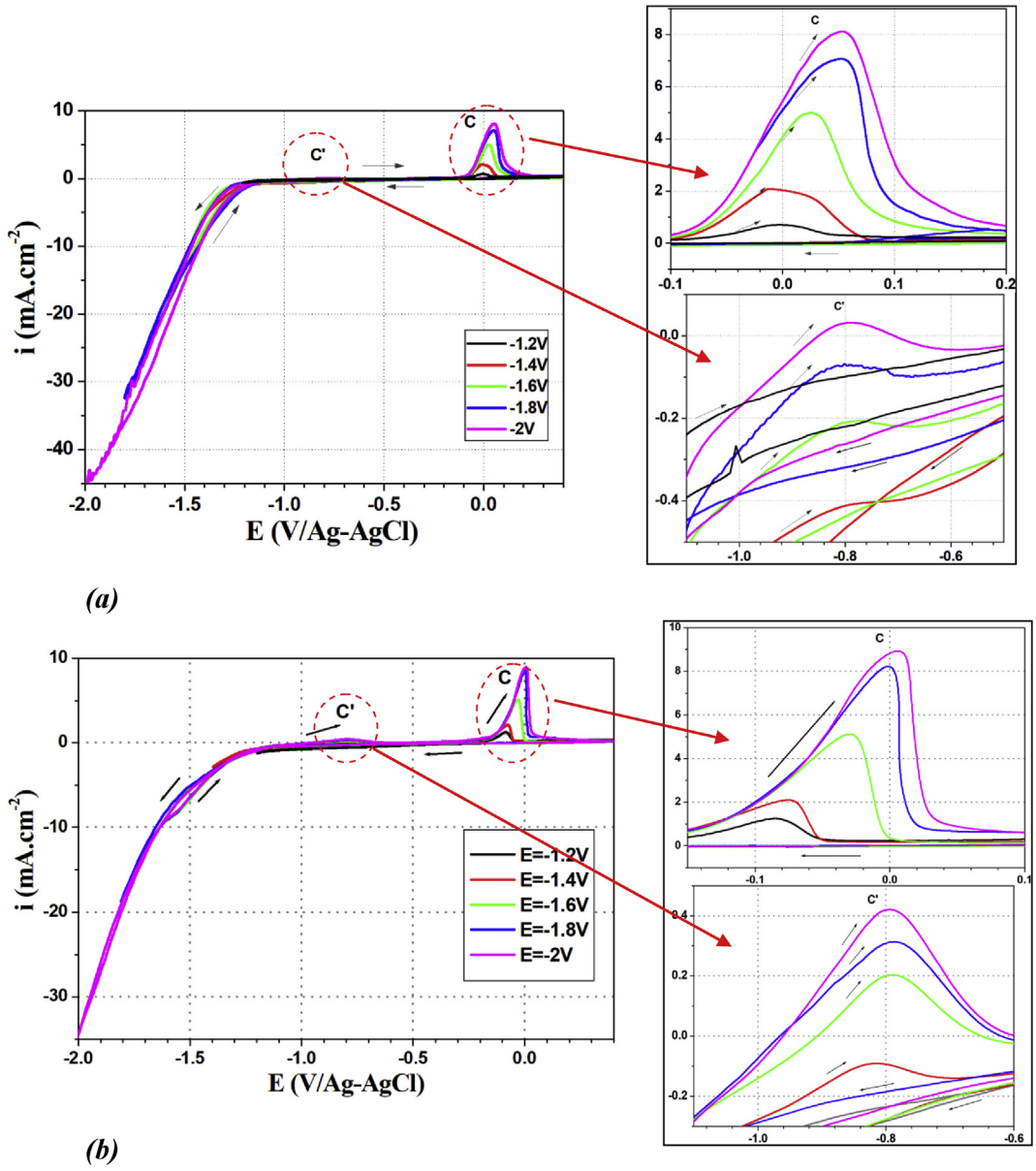

Fig. 2. Cyclic Voltammograms recorded on GC electrode in (a) sulphate (S3) and (b) chloride (S6) baths, for different cathodic switching potentials, $S_R = 20$ mV s^{-1}, $\Omega = 250$ rpm, with the highlights of the peaks.

Most of the reported baths for Cu–Zn electrodeposition are sulphate based and rarely chloride. Ballesteros et al. have electrodeposited copper [34], zinc [35] and Cu–Zn [1] on nickel from chloride baths containing glycine. They observed a dependence of the faradic current efficiency and the surface morphology of these deposits on the electrolyte composition and applied potential. They obtained higher faradic current efficiency at -1.35 *V vs.*(*SCE*) (77%) than that obtained at -1.5 *V vs.*(*SCE*) (63%), which was explained by the contribution of HER. At more cathodic potential, the faradic current efficiency increases due to high amount of zinc, which inhibits the hydrogen evolution reaction. Current efficiency was improved when Zn was increased and different intermetallic phases were formed at potentials less than -1.5 *V vs.*(*SCE*) while at potentials above -1.5 *V vs.*(*SCE*) α-phase was formed principally.

A comparative study highlighting the effect of chloride and sulphate anions has not been reported yet for Cu–Zn. The aim of this work is to discuss the influence of anions type on Cu–Zn electrodeposition from citrate-based electrolytes. The impact on the hydrogen evolution reaction and consequently on the cathodic current efficiency as well as on the alloy coatings morphology, is evaluated.

2. Experimental

Cu, Zn and Cu–Zn alloys were electrodeposited from chloride and sulphate baths with the composition given in Table 1. All plating baths were prepared using SIGMA-ALDRICH products (≥99%) and double distilled water. Two different anions (sulphate and chloride) were used for the comparison. Sulphate electrolytes contain zinc sulphate (S1) or/and copper sulphate (S2, S3) while chloride baths contain zinc chloride (S4) or/and copper chloride (S5, S6). Both sulphate (S1, S2 and S3 solutions) and chloride (S4, S5 and S6 solutions) baths, contain trisodium citrate ($Na_3C_6H_5O_7.2H_2O$) as a source of citrate ligand ($Cit^{3-} = C_6H_5O_7^{3-}$), boric acid ($H_3BO_3$) to decrease the hydrogen evolution reaction (HER), to improve the morphology of the electrodeposited film and to serve as a buffer by controlling the pH [32, 36, 37, 38]. Sodium saccharin ($C_7H_4\ NNaSO_3.H_2O$) is added to reduce the internal stress in the coating by providing a suitable crystallization and a regular structure to the deposit. Hence, it favors fine grains growth to achieve a shiny, bright and adherent coating [39, 40]. Sodium sulphate (Na_2SO_4) and

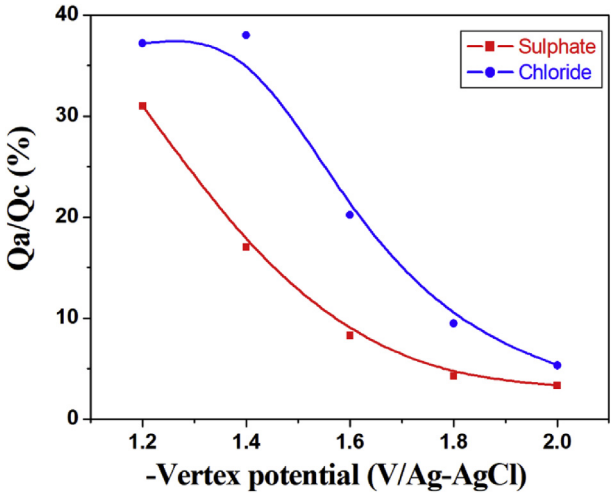

Fig. 3. Current efficiency of Cu–Zn deposition as a function of the switching potential in sulphate (S3) and chloride (S6) bath.

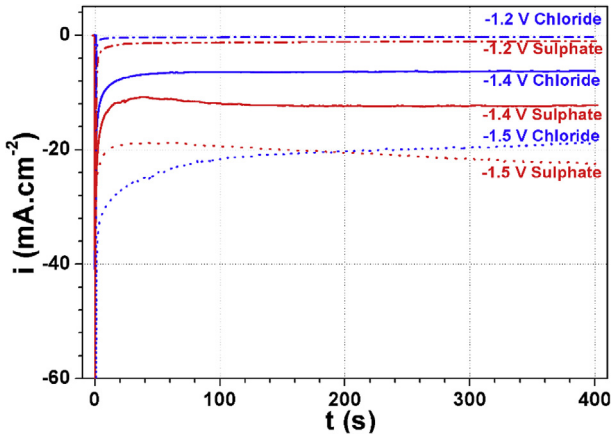

Fig. 4. Current-time transient curves of Cu–Zn deposition on steel substrate recorded at different potentials during 400s in sulphate (S3) and chloride (S6) baths.

potassium chloride (KCl) are used as supporting electrolytes in sulfate and chloride baths, respectively. The concentrations of these chemicals given in Table 1, are similar in chloride and sulphate baths. The pH of both baths was about 6. For the kinetic study, electrodeposition of individual Zn and Cu coatings have been performed from (S1 or S4) and (S2 or S5) solutions, respectively.

Electrochemical measurements were performed using a potensiostat/galvanostat PGSTAT30 (AUTOLAB) controlled by Autolab Software version 4.8 and connected to a three-electrode electrochemical cell. An Ag /AgCl electrode saturated with KClis used as reference electrode ($E = 0.197\ V\ vs.\ SHE$) and platinum plate (1.1 cm^2) as counter electrode. Glassy carbon (GC) rotating disc electrode (S = 0.2 cm^2) with a rotation speed Ω = 250 rpm, was used as working electrode for the kinetic study while carbon steel of DC01 grade (S = 0.4 cm^2) was used for Cu–Zn electrodeposition at constant potential.

Before each experiment, the working electrodes was pretreated as follow: GC was pickled in a dilute solution of nitric acid, then degreased in ethanol under ultra-sonication, rinsed with distilled water and finally dried under nitrogen stream prior to use. The carbon steel substrate was mechanically polished on SiC papers (2000 grades) under water jet. To achieve mirror finish surface, the substrate is further polished with diamond paste down to 1 μm size. Finally, it is ultra-sonicated for 10 minutes in ethanol and then rinsed with distilled water. To improve the adherence of the coating, the surface of the steel substrate is activated by immersing it for a few seconds in a HCl solution. The etching process increases the surface roughness which allows the coating to cling to the surface of the substrate.

The kinetic study of the electrodeposition of Cu, Zn and Cu–Zn on GC electrode, was achieved by cyclic voltammetry (CV) with a scan rate $S_R =$ 20 mV/s. The chronoamperommetry (CA) method is used for Cu–Zn electrodeposition on carbon steel at different potentials and constant duration time t = 400 s. All measurements were carried out at room temperature. Before each experiment, the solution was deaerated by bubbling pure nitrogen during 30 min, which is stopped during the electrodeposition measurements. The corrosion resistance tests of the coated and uncoated steel were carried out by linear sweep voltammetry after 15 min of open circuit potential (OCP) measurement in aerated 0.5 M NaCl aqueous solution of pH = 6.5 at scan rate $S_R = 1\ mV.s^{-1}$.

The surface morphology and chemical composition of the deposits are performed using a Philips LS30 scanning electron microscope (SEM) equipped with energy dispersive X-ray (EDS). The crystalline phases study of the coating is carried out with the help of Panalytical X'PERT PRO diffractometer with monochromatic CuKα radiation. XPS spectra were measured on a Thermo Scientific K-Alpha spectrometer using a monochromatized X-ray *K*α radiation (1486.6 eV); the photoelectrons collected at 0° with respect to the surface normal were analyzed using a hemispherical analyzer. A general spectrum (survey) was collected for each alloy. The C (1s) line of adventitious carbon at 285 eV binding energy was used to normalize the absolute binding energies. Surface sputtering or bombardment by Ar^+ ions was used for depth profiling with an energy level of 500eV during 10s. XPS survey spectra were used after the second etching and analyzed by Thermo Advantage software, version 5.967.

3. Results and discussions

3.1. Analysis of cyclic voltammograms

Fig. 1 shows the cyclic voltammograms recorded on GC substrate in sulphate and chloride citrate based baths presented in Table 1. The potential was scanned from the rest potential towards the negative direction between −1.5 and + 0.4 $V\ vs.(Ag/AgCl/KCl)$, at a scan rate $S_R = 20\ mV.s^{-1}$. Figs. 1a and b shows the cyclic voltammograms recorded for Cu, Zn and Cu–Zn in sulphate and chloride baths. The voltammograms display a plateau of a weak cathodic current attributed to the metal depositions under diffusion control. Up to about − 1.2 $V\ vs.(Ag/AgCl/KCl)$, a sharp rise is noted, corresponding to the competitive hydrogen evolution reaction (HER):

$$H^+ + e^- \rightarrow \frac{1}{2}H_2 \quad (5)$$

At pH = 6, the theoretical reversible potential of HER is:

$$E_{eq.H_2} = -\ 0.06\ pH = -\ 0.366\ V\ vs.(SHE) = -\ 0.563\ Vvs.(Ag/AgCl/KCl) \quad (6)$$

But the potential at which HER starts on GC electrode, is generally more negative than the reversible potential (− 0.563 $V\ vs.(Ag/AgCl/KCl)$. This potential difference, depends on the nature of the electrode material.

In the reverse scan, current peaks (A, B, C and C') appear and can be attributed to Zn, Cu and Cu–Zn dissolutions, respectively, according to voltammogramms of each element (Fig. 1) and to the theoretical reversible potentials.

The zinc or copper can electrodeposits from the main stable forms of M-citrate complexes at pH = 6, according to the following reactions [38, 47, 48, 49].

$$ZnCit_2^{4-} + 2e^- \rightarrow Zn + 2Cit^{3-} \quad (7)$$

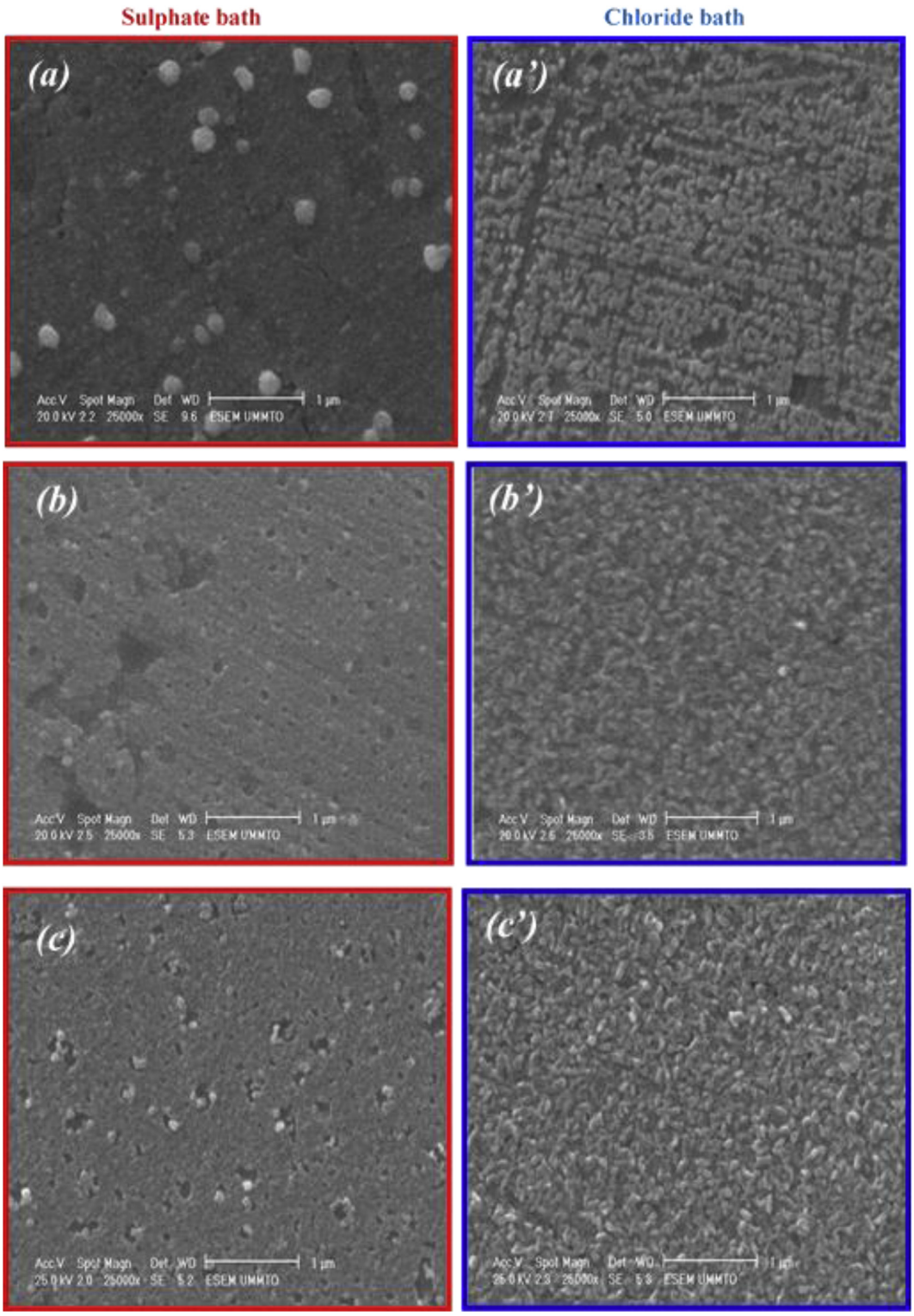

Fig. 5. SEM micrographs of Cu–Zn deposits at (a) – 1.2 V vs.(Ag/AgCl/KCl), (b) – 1.4 V vs.(Ag/AgCl/KCl), (c) – 1.5 V vs.(Ag/AgCl/KCl), from sulphate and chloride baths during 400 s.

$$Cu_2Cit_2^{2-} + 4e^- \rightarrow 2Cu + 2Cit^{3-} \quad (8)$$

The stability constants for Zn-Citrate and Cu-Citrate complexes are [50, 51, 52, 53]:

$$Zn^{2+} + 2Cit^{3-} \leftrightarrow ZnCit_2^{4-} \qquad Log\beta = 5.9 \quad (9)$$

$$2Cu^{2+} + 2Cit^{3-} \leftrightarrow Cu_2Cit_2^{2-} \qquad Log\,\beta' = 17.3 \quad (10)$$

In the test conditions of pH and concentrations of the baths shown in Table 1, the deposition of the nobler metal is favored and Cu-rich coatings are produced.

The equilibrium potential below which each metal, zinc or copper, can be electrodeposited from the complex ions, is calculated using Nernst equation:

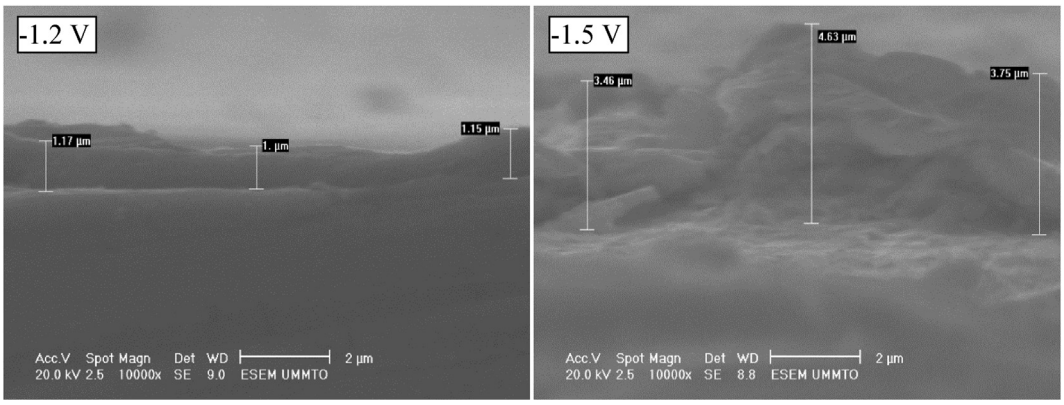

Fig. 6. SEM cross-section image of Cu–Zn deposit prepared at −1.2 V and −1.5 V from chloride bath (S6) during 20 min.

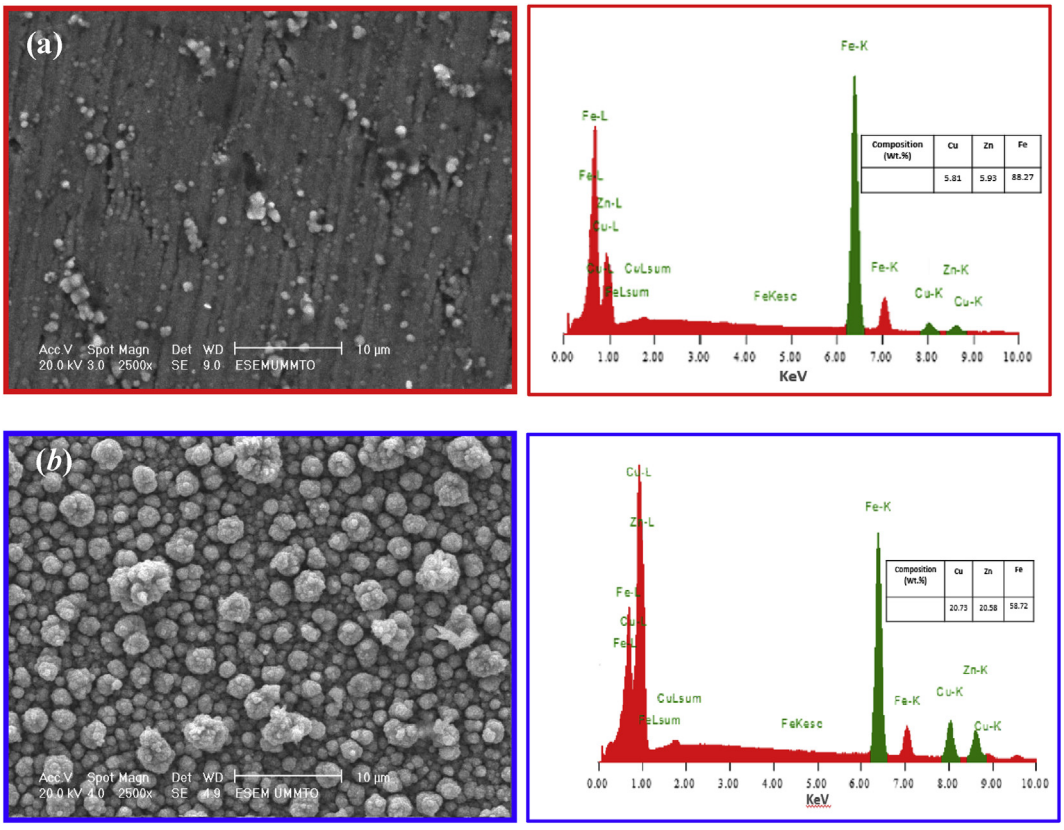

Fig. 7. SEM micrographs and EDS analysis of Cu–Zn deposit on steel substrate, at −1.4 V vs.(Ag/AgCl/KCl) for 20 min, from a) sulphate and b) chloride bath.

$$E_{eq,M^{2+}/M} = E^{0}_{M^{2+}/M} + 0.03\,Log\left(\left[M^{2+}\right]\right) \tag{11}$$

Using the following concentration of each metal,

$$\left[Zn^{2+}\right] = \frac{\left[ZnCit_2^{4-}\right]}{\beta\left[Cit^{3-}\right]^2} \text{ and } \left[Cu^{2+}\right] = \frac{\left[Cu_2Cit_2^{2-}\right]^{1/2}}{\beta^{1/2}\left[Cit^{3-}\right]} \tag{12}$$

with the concentrations: $[Cit^{3-}] = [Cit^{3-}]_0 - [MCit^-]$ and $[MCit^-] = [M^{2+}]_0$ and the standard potentials: $E^{0}_{Zn^{2+}/Zn} = -0.76\ V\ vs.SHE$ and $E^{0}_{Cu^{2+}/Cu} = 0.34\ Vvs.SHE$,

Eq. (11) become for Zn or Cu:

$$E_{eq,Zn^{2+}/Zn} = E^{0}_{Zn^{2+}/Zn} - 0.03\,Log(\beta) + 0.03\,Log\left(\frac{\left[ZnCit_2^{4-}\right]}{\left[Cit^{3-}\right]^2}\right) = -1.1823\ V\ vs.(Ag/AgCl/KCl) \tag{13}$$

$$E_{eq,Cu^{2+}/Cu} = E^{0}_{Cu^{2+}/Cu} - 0.03\,Log\left(\beta^{'1/2}\right) + 0.03\,Log\left(\frac{\left[CuCit^-\right]^{1/2}}{\left[Cit^{3-}\right]}\right) = -0.138\ V\ vs.(Ag/AgCl/KCl) \tag{14}$$

In a first case, Zn and Cu electrodepositions are studied separately. The zinc electrodeposition is conducted from S1 and S4 solutions, showed in black in Fig. 1a and b, respectively. A cathodic diffusion-limited plateau is observed in the potential range [−0.85 to −1.25 *V vs.*(*Ag/AgCl/KCl*)], it is the limiting current region of an amplitude $i_{L,Zn} = -0.37\ mA/cm^2$, where Zn(II) reduction occurs under mass

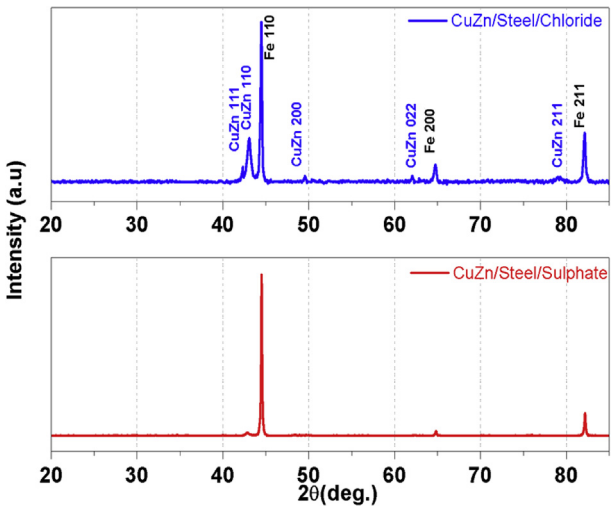

Fig. 8. XRD patterns of Cu–Zn alloy electrodeposited on steel substrate from sulphate and chloride bath at −1.4 V vs.(Ag/AgCl/KCl) for 20 min.

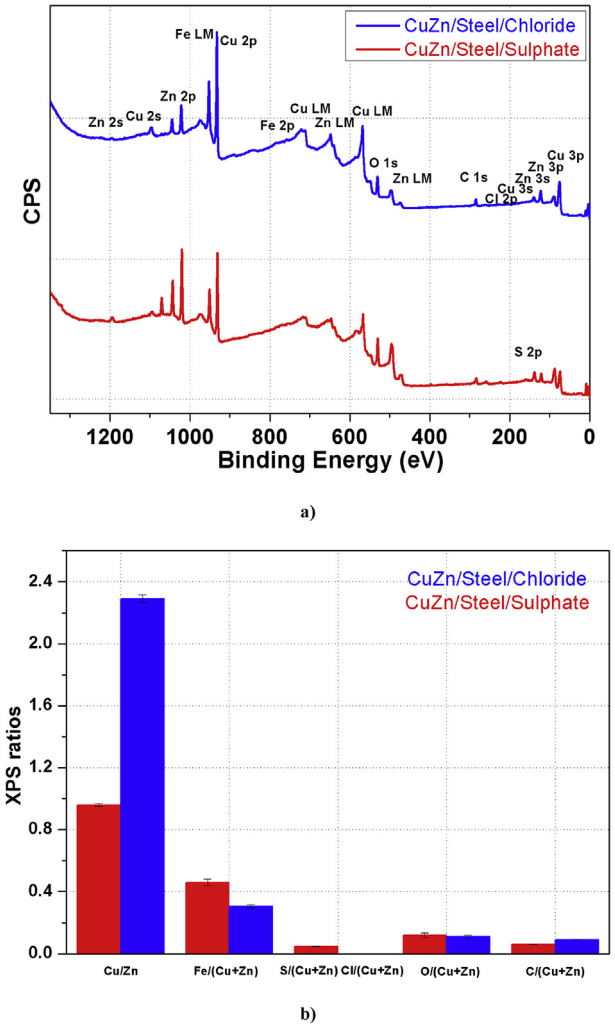

Fig. 9. XPS survey spectrum (a) and rations (b) of Cu–Zn alloy obtained from chloride and sulphate baths at −1.4 V vs.(Ag/AgCl/KCl) during 20 min.

transport control. A sharp increase in current density of Zn electrodeposition at − 1.3 *V vs.*$(Ag/AgCl/KCl)$, indicates an increase in the overvoltage of the hydrogen evolution reaction (HER) on previously deposited Zn and occurs simultaneously with the reduction of Zn^{2+} ions on GC. The reverse scan intercepts the potential axis at a same value of − 1.1 *V vs.*$(Ag/AgCl/KCl)$ for sulphate (S1) and chloride (S4) which is related to the equilibrium potential of redox couple Zn(II)/Zn, very close to the calculated thermodynamic potential (in Annex), in agreement with Mendoza-Huizar et al. [41]. In the anodic part, a principal peak A appearing at $E_p = -1.05$ *V vs.*$(Ag/AgCl/KCl)$ for both Zn plating baths, is attributed to the dissolution of the previously deposited Zn. Thus, we notice that the anion type has no effect on the E_p value of Zn.

While in the case of copper electrodeposition from (S2) and (S5) baths (Fig. 1a and b, respectively), a cathodic diffusion-limited plateau, $i_{L,Cu}$, of a similar amplitude as for zinc deposition, is observed in the potential range −0.6 to − 1.05 *V vs.*$(Ag/AgCl/KCl)$. It is associated to the complex cupric ions reduction. A sharp increase in cathodic current density at − 1.05 *V vs.*$(Ag/AgCl/KCl)$ is related to HER. In the reverse scan direction, the curve intercept the potential axis at −0.25 and − 0.3 *V vs.*$(Ag/AgCl/KCl)$in S2 and S5 solutions, respectively, which is close to the thermodynamic equilibrium potential of the redox couple Cu(II)/Cu (in Annex). The anodic peak B observed at 0.05 and − 0.03 *V vs.*$(Ag/AgCl/KCl)$ (in S2 and S5 solutions, respectively), is related to the Cu dissolution.

In the second case, Cu and Zn are co-deposited from sulphate (S3) and chloride baths (S6), respectively. Analysis of the blue curves shown in Fig. 1a and b, indicates a diffusion limit current ($i_{L,CuZn}$) twice as high as those observed for individual copper and zinc which originates from the sum ($i_{L,Zn} + i_{L,Cu}$) . During the anodic scan two anodic peaks (C and C′) appear and lie between Zn and Cu peaks (A and B, respectively). Peak C is the major anodic signal and it is obtained at ≈ 0 and −0.06 *V vs.*$(Ag/AgCl/KCl)$ (from S3 and S6), a value, which is closer to that of Cu dissolution, but slightly at lower potential and peak C′ at − 0.8 *V vs.*$(Ag/AgCl/KCl)$, closer to the potential of Zn peak (A). Peak C is attributed to the dissolution of a codeposited Cu–Zn film and supports the hypothesis of an electrodeposition of Cu–Zn alloy rich in copper. The peak C′ can be associated with dissolution of Cu–Zn alloy rich in zinc, in agreement with Ballesteros et al. [1]. The peak C corresponds to the dissolution of the α-phase of Cu–Zn alloy, which forms first and in much higher quantities than the zinc rich ε-phase. That is the reason for higher intensity of the peak C in comparison with that of peak C' zinc rich ε-phase. Consequently, the current efficiency of Cu deposition is higher than that of Zn as mentioned above.

For the comparison between CVs performed from sulphate and chloride baths, Fig. 1c, d and e, highlight the influence of anion nature.

The cathodic branches of CVs in presence of Cl^- anions (in blue) are shifted to the right (the anodic potentials) compared to those in sulphate solutions. According to Rudnik [33], sulphate anions inhibit cathodic reaction due to their adsorption on the electrode surface, which is not the case with chloride anions.

In chloride baths, crossovers between the forward and the reverse scan are observed around −1 *V vs.*$(Ag/AgCl/KCl)$ for Cu and −1.2 *V vs.* $(Ag/AgCl/KCl)$ for Zn and Cu–Zn deposits, which characterizes new phases formation [41]. When the potential was reversed, the curve is shifted to less negative potentials since the potential of Zn or Cu deposition become more positive (low overpotential) because it takes place on a less surface of previously deposited Zn or Cu. This type of profile, known as hysteresis current loop [42], indicates a formation of nucleation centers.

On the anodic part of the voltammograms, peaks appear with higher current densities in chloride bath, as reported in Table 2, indicating that the type of anions in the bath influenced the rate of the process. Enhanced electrodeposition in chloride system can be a consequence of the higher conductivity of the chloride solution (60 mS/m) compared to sulphate bath (49 mS/m). In addition, at high chloride concentration, formation of chloride layer may be in competition with citrates complexes of the metallic ions. In agreement with several authors [31, 33, 43], the formation of complexes between metallic cations and chloride anions can

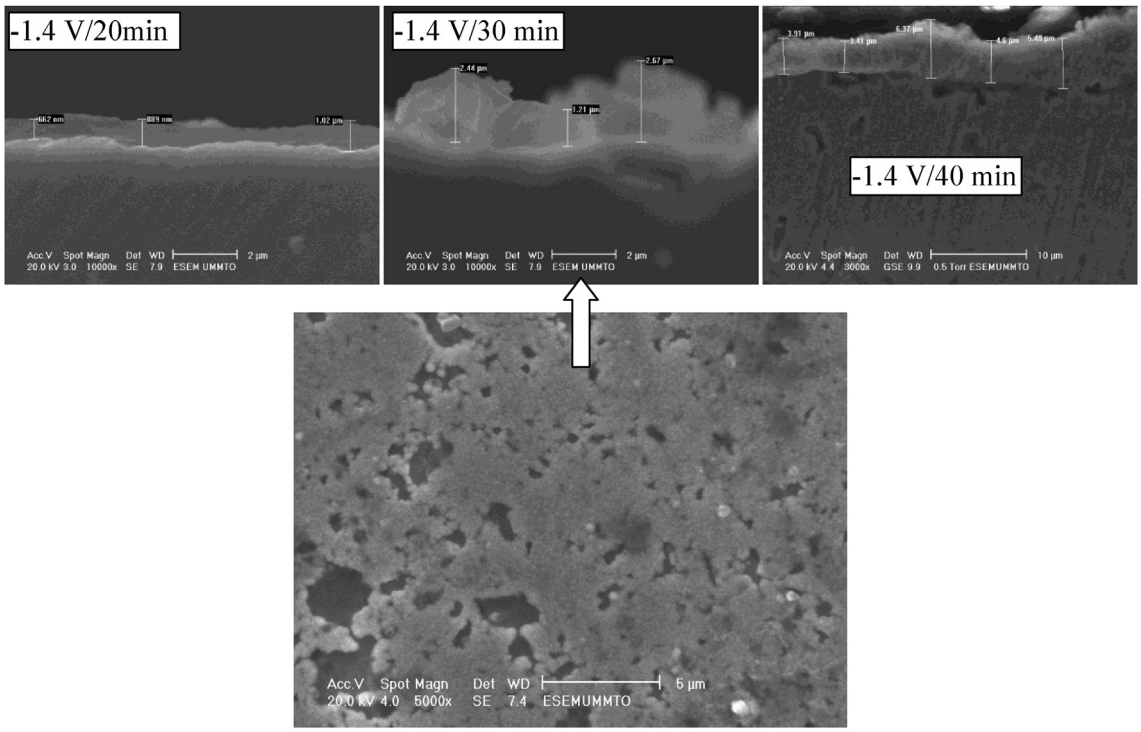

Fig. 10. SEM cross-section image of Cu–Zn deposit prepared at −1.4 V from sulphate bath (S3).

activate the electrodeposition process leading to a higher production of alloy deposit which can inhibit HER. On the other hand, adsorption of sulphate anions may inhibit the cathodic process, as reported by Rudnik [33].

We can notice that the dissolution potential of peak C' (Cu–Zn rich in Zn) was not affected by the nature of the anions, as for peak A (individial Zn electrodeposition), while the potential of peak C (Cu–Zn rich in Cu) was shifted to more negative values in presence of chloride anions, in agreement with the previous discussions. This behavior can be ascribed to a change in the composition of the Cu–Zn alloy rich in Cu (peak C) by an increase in quantity of copper while Cu–Zn rich in Zn (peak C') is related to an increase in quantity of zinc.

3.1.1. *Influence of the switching potential*

The effect of the switching potential (potential at which scan direction is reversed) on the kinetics of Cu–Zn electrodeposition is studied, based on a series of CVs, displayed in Fig. 2. The voltammograms are recorded on GC electrode, scanned in the negative direction until different potential values (from −1.2 to − 2 *V vs.*(*Ag*/*AgCl*/*KCl*)) and afterwards scanned in the reverse direction.

The switching potential influences strongly the shape of the voltammograms. Indeed, as can be noticed on the voltammograms recorded from S3 and S6, crossovers appears in the forward scan which characterize the formation of new phases, accompanied by an increase in the peaks area. For voltamograms obtained at low switching potentials and very low charges, small oxidation peaks C and C' were noticed at more negative peak potentials, as highlighted in Fig. 2.

In the chloride bath shifting of the anodic peak C towards more positive potentials were observed as the switching potential becomes more negative. This observation indicates evidently a change in the composition of the deposit assuming an increase in copper content, in agreement with Ballesteros et al. [1].

Fig. 3 displays the Faradic current efficiency, *R*, which is obtained using the ratio between the anodic and the cathodic charges, associated with anodic and cathodic total currents. The charges were determined by integrating the different voltammograms, using the following relationships:

$$Q = \int I.\, dt \tag{15}$$

$$R\,(\%) = \frac{Q_a}{Q_c} \times 100 \tag{16}$$

Q_c: is the total cathodic charge which is used for the reduction reactions of Cu^{2+}, Zn^{2+} and H^+, associated to the total reduction current density given by:

$$i_c = i_{c,Cu} + i_{c,Zn} + i_{c,H2} \tag{17}$$

Q_a: is the total anodic charge, which serves only for Cu–Zn dissolution reaction with the total anodic current density given by:

$$i_a = i_{a,Cu} + i_{a,Zn} \tag{18}$$

Current efficiency values decrease when the switching potential is more negative. In all cases, the efficiency values are less than 100% due to the contribution of the HER which increases with the switching potential, in agreement with Ballesteros et al. [1].

The maximum current efficiency is obtained at the switching potential −1.2 V, beyond which HER is observed. At this potential, the copper reduction is significant because peak C' is absent, indicating negligible amount of Zn, as highlighted in Fig. 2, since the applied potential is very distant from Cu equilibrium potential but is closer to the Zn equilibrium potential.

As the switching potential becomes more negative, the current efficiency decreases, but remains higher in chloride solution than that in sulphate. An increase in Zn content from chloride bath is evidenced by the increase of peak C' when the switching potentials are more negative. This fact is attributed to the catalytic effect of chlorides and to the adsorption effect of sulphate anions, as mentioned before. In addition, the use of chloride anions increases the conductivity of the electrolyte, consequently the rate of the overall process increases.

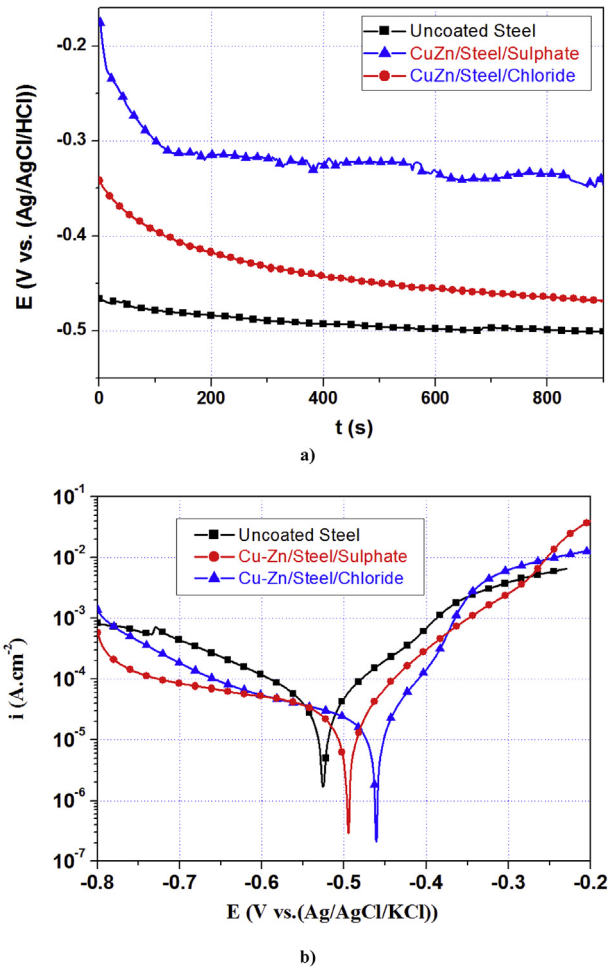

Fig. 11. Electrochemical characterizations of steel and Cu–Zn electrodeposited on steel from sulphate and chloride baths: (a) OCP vs. time and (b) polarization curves at $S_R = 1$ mV/s after 15 min in 0.5 M NaCl solution.

Table 3
Corrosion parameters values of Cu–Zn coatings and steel obtained from the polarization curves in Fig. 11.

Sample	OCP (V vs. (Ag/AgCl/KCl))	E_{corr} (V vs.(Ag/AgCl/KCl))	i_{corr} (μA/cm^2)
Uncoated Steel	−0.52	−0.55	42
Cu–Zn/Steel/ Sulphate bath	−0.46	−0.49	28
Cu–Zn/Steel/ Chloride bath	−0.35	−0.45	19

3.2. Potentiostatic deposition of Cu–Zn

Cu–Zn alloy coatings were electrodeposited on steel substrates, from sulphate and chloride baths (S3 and S6 respectively), at − 1.2, −1.4 and − 1.5 *V vs.*(*Ag*/*AgCl*/*KCl*). Fig. 4 shows the as recorded chronoamperograms (CA) of increasing deposition potential in the two different baths. As observed, nearly similar shape was found for the different curves. Two zones which are related to different physical phenomena can be clearly distinguished. The first one happens at a short time (<0.5 s), where a sharp increase in the cathodic current densities, corresponds to the discharge of a double layer and the formation of the first nucleation centers of Cu–Zn. In the second zone, the current density decreases, characterizing the growth step of the nuclei. Further increase of the deposition time leads to the stabilization of the current density.

For both baths, shift of the applied potential to more negative values, increases the resulting current density, which can be due to the increase of the deposition rate and to the HER contribution, which becomes more important, in agreement with the decrease in the current efficiency of the process. At − 1.4 *V vs.*(*Ag*/*AgCl*/*KCl*), the current density is four times larger than for the deposition carried out at − 1.2 *V vs.*(*Ag*/*AgCl*/*KCl*). This highly affects the process, as shown by the morphological characterization (Fig. 5). The comparison between the transients obtained in the two baths at different deposition potentials, shows higher current density in the sulphate bath (S6) at any applied potential. This can be explained by the higher adsorption capacity of sulphate ions due to their high affinity to the substrate surface which reduces the deposit thickness and then points to the formation of a less protective film.

This is attributed to the formation of chloride complexes in chloride citrate bath in addition to the inhibiting effect of the sulphate anions. The result is in agreement with the current efficiency values (high values in the chloride bath).

The SEM micrographs presented in Fig. 5 show the dependence of the morphology of the Cu–Zn coated steel on the applied potential and on the type of anion in the plating baths (S3 and S6).

It was found that deposition at −1.2 *V vs.*(*Ag*/*AgCl*/*KCl*) (Figs. 5a and a'), leads to a slight surface coverage in which nucleation and growth of Cu–Zn coating occurred only at favorable sites on the steel surface. At − 1.5 *V vs.*(*Ag*/*AgCl*/*KCl*) (Fig. 5c and c') the deposit was intensified and overlapping over the whole steel surface.

Thicknesses of Cu–Zn deposits were estimated from SEM cross-section. Fig. 6 shows in the inset word boxes a thickness of an average value 1.1 μm produced at −1.2 *V vs.*(*Ag*/*AgCl*/*KCl*) and 3.95 μm produced at − 1.5 *V vs.*(*Ag*/*AgCl*/*KCl*).

From sulphate bath, finer grained and porous deposits were observed with surface irregularity and less adherence film (estimated manually), accompanied by worsening of the quality of the Cu–Zn layers at more negative potential attributed to HER.

On the other hand, the deposit obtained from chloride bath has homogeneous, compact morphology and bigger grain size. When plating potential become more negative, mass of the deposit increases, grain shape changes from spherical to flaky and the grain size increases. These observations are in perfect agreement with the above analysis of the electrochemical results.

Based on this optimization, Cu–Zn alloys are deposited from chloride bath at −1.4 *V vs.*(*Ag*/*AgCl*/*KCl*). Moreover, in order to increase the thickness as well as the covering of the steel surface, the electrodeposition time is increased to 20 min and the Cu–Zn alloys present a bright golden color.

The SEM micrographs for Cu–Zn deposit, obtained in these conditions, are shown in Fig. 7a and 7b. For each of the deposits, EDS analyses were carried out in order to assess the composition of Cu–Zn deposits on steel.

The EDS results indicate that Cu–Zn amount obtained from chloride (Fig. 7b) bath was higher than that deposited from sulphate bath (Fig. 7a). From Fig. 7b, it appears that the alloy is composed of defined granules with definite boundaries and a cauliflower form, distributed on each other with an average particle size equal to 1.5 μ*m* while the alloy formed from sulphate bath is not covering the entire substrate area.

X-ray diffraction analysis was performed in order to determine the crystalline orientations of the Cu–Zn alloys. Fig. 8 shows the obtained XRD patterns the dominate phases of the Cu–Zn coating on steel substrate at −1.4 *V vs.*(*Ag*/*AgCl*/*KCl*) during 20 min.

The characteristic peaks of the Cu–Zn alloy have been well demonstrated in chloride bath compared to sulphate bath where the substrate peaks are predominant. This can be due to the fact that the substrate was not uniformly covered with Cu–Zn alloy and also to a small thickness of the deposit. These results are in line with SEM images obtained in Fig. 7.

According to Juskenas et al. [22] for Cu–Zn deposited from sulphate D-mannitol bath, the α-(Cu–Zn) phase started to form at −1.2 *V vs.*(*Ag*/*AgCl*/*KCl*) with 1% of Zn and at potential −1.495 *V vs.*(*Ag*/*AgCl*/*KCl*) 30.7% Zn was reached and peaks of β, γ and ε phases emerge on the XRD

patterns.

Balesteros *et al.* [1] reported that since Zn is deposited via an underpotential deposition (UPD) process, the electrodeposition of Cu–Zn alloy results in a mixture of multiphase composition of the alloy.

Fig. 9a and b show the XPS survey of Cu–Zn deposited from chloride and sulphate baths at $-1.4\ V\ vs.(Ag/AgCl/KCl)$ for 20 min and the overall atomic ratios obtained from the survey spectra (b) taken in wide kinetic energy range. The observed peaks assigned to C1s, O1s, Cu (2p, s and LMM), Fe (2p, 3s and LMM), Zn (2p, s and LMM), Cl (2p) and S (2p) [44]. The surface Cu/Zn atomic ratio from chloride bath is determined to be 2.29 while it is 0.96 from sulphate bath. The O1s and C1s adsorbed brass surfaces are in small amount, the O/Cu–Zn ratios are 0.10 and 0.12 from chloride and sulphate baths respectively and the C/Cu–Zn ratios are 0.09 and 0.06, this is due to the contaminants, which cannot be eliminated after the first etching at 500 eV. Note that we cannot exclude the possibility of contribution of OH to the O1s peaks observed at 531.4, as the O1s peak of OH can be expected in this energy region [45].

The Fe/(Cu + Zn) ratio obtained from sulphate bath is higher than in chloride bath (Fig. 9b), these results are in line with the SEM observations obtained from Fig. 7. In addition, S/(Cu + Zn) ratio is obtained from the sulphate bath which can confirm the previous discussions and the adsorption effect of sulphate anions on the alloy surface.

3.3. Electrochemical characterizations

The corrosion resistance of Cu–Zn alloy deposited at $-1.4\ V\ vs.(Ag/AgCl/KCl)$ was evaluated by potentiodynamic polarization in an aerated 0.5 M NaCl solution of pH = 6.5. In order to increase thickness of the deposits from sulphate (S3), deposition time was increased from 20 min to 40 min (Fig. 10). Approximately a same thickness was produced for 20 min from chlorides and for 30 min from sulphate.

Fig. 11a and b, show OCP decay and polarization curves of coated and uncoated steel substrates.

The OCP curves for both Cu–Zn coatings evolve in decreasing towards a stationary state, characterized by a more positive potential value than the substrate (steel), which means that Cu–Zn coating is electrochemically cathodic with respect to the steel substrate. The ennobling of Cu–Zn OCP, compared to steel, is probably related to a high copper amount in the deposit.

The shift of OCP towards the corrosion potential of the substrate indicates a behavior of galvanic coupling between the steel and the coating, where steel is an anode relative to brass. The corrosion is initiated on the low Cu–Zn covered areas and propagates under the coating giving formation to porous layers [46]. By comparing the OCP of the two coatings, Cu–Zn electrodeposited from chloride presents the more positive value; hence, it provides better recovery, which is in agreement with SEM analysis.

The potentiodynamic polarization curves of Cu–Zn coated and uncoated steel are shown in Fig. 10b. A similar shape is observed for all curves, corresponding to the hydrogen evolution reaction from the solvent in the cathodic domain followed by Cu–Zn and steel substrate dissolutions. Cu–Zn curves were shifted towards more positive potentials, compared to uncoated steel, indicating a protecting effect of the steel by the Cu–Zn film. For comparison between the two plating baths, it is interesting to note that Cu–Zn produced from chloride bath presents a more positive value of E_{corr} than that produced from sulphate bath.

The corrosion current densities, i_{corr}, values given in Table 3, were determined using Tafel extrapolation method. It appears from the values that the corrosion resistance of the coated steel increases compared to the uncoated steel. The i_{corr} values decrease in the following order:

$$i_{corr}\ (uncoated\ Steel) > i_{corr}\ (Cu-Zn/Steel/sulphate) > i_{corr}\ (Cu-Zn/Steel/chloride)$$

The lowest value of i_{corr} was obtained for the coating produced from chloride bath which means a higher anti-corrosion performance in the aggressive medium, comparatively to the Cu–Zn formed from sulphate bath which may not protect the steel efficiently. The result is in agreement with the deposit current efficiency and the SEM characterizations.

4. Conclusions

Electrodeposition of Cu–Zn alloys from chloride and sulphate baths were investigated by various techniques. The following conclusions were obtained from the experimental conditions of the study, namely at pH = 6 and at a high citrate concentration in the baths.

- Higher current efficiency of the Cu–Zn co-deposition is obtained in chloride solutions, compared to sulphate baths. The above phenomena can be attributed to the catalytic effect of chloride anions by increasing conductivity and to the weaker adsorption capacity of chloride with respect to sulphate ions. In addition, at the high chloride concentration, formation of chloride layer may be in competition with citrates complexes in the reduction process of the metallic ions, while the cathodic inhibiting effect of adsorbed sulphate anions decreases metallic reductions.
- Potentiostatic study indicates that Cu–Zn deposits, obtained from chloride, are thicker, in agreement with the SEM morphological characterization.
- Corrosion of CuZn in 0.5 M NaCl solution leads to ennobling OCP value of the Cu–Zn alloys obtained at $-1.4\ V\ vs.(Ag/AgCl/KCl)$ when compared to steel. Cu–Zn deposit produced from chloride bath presents higher corrosion resistance.
- The results of several techniques are in good agreement.

Declarations

Author contribution statement

C Oulmas: Performed the experiments; Analyzed and interpreted the data; Wrote the paper.

S. Mameri: Performed the experiments.

D. Boughrara: Conceived and designed the experiments; Analyzed and interpreted the data; Contributed reagents, materials, analysis tools or data; Wrote the paper.

A. Kadri: Conceived and designed the experiments; Analyzed and interpreted the data; Contributed reagents, materials, analysis tools or data.

J. Delhalle: Contributed reagents, materials, analysis tools or data.

Z. Mekhalif: Analyzed and interpreted the data; Wrote the paper.

B. Benfedda: Analyzed and interpreted the data.

Funding statement

This work was supported by the Laboratoire de Physique et Chimie des Matériaux (LPCM), Université Mouloud MAMMERI de Tizi-Ouzou (UMMTO) of Algeria and the Laboratoire de Chimie et d'Electrochimie des Surfaces (CES), Université de Namur of Belgium, through the financial support of Département de Chimie de la Faculté des Sciences of UMMTO and the project "Erasmus+".

Competing interest statement

The authors declare no conflict of interest.

Additional information

No additional information is available for this paper.

References

[1] J.C. Ballesteros, L.M. Torres-Martínez, I. Juárez-Ramírez, G. Trejo, Y. Meas, Study of the electrochemical Co-reduction of Cu^{2+} and Zn^{2+} ions from an alkaline non-cyanide solution containing Glycine, J. Electroanal. Chem. 727 (2014) 104–112. Elsevier B.V.

[2] A.D.S. Taguchi, F.R. Bento, L.H. Mascaro, Nucleation and growth of tin-zinc electrodeposits on a polycrystalline platinum electrode in tartaric acid, J. Braz. Chem. Soc. 19 (2008) 727–733.

[3] E.M. de Oliveira, I.A. Carlos, Chemical, physical and morphological characterization of ZnNi films electrodeposited on 1010 steel substrate from acid baths containing polyalcohol, Surf. Coating. Technol. 206 (2011) 250–256. Elsevier B.V.

[4] C. Savall, C. Rebere, D. Sylla, M. Gadouleau, P. Refait, J. Creus, Morphological and structural characterisation of electrodeposited Zn-Mn alloys from acidic chloride bath, Mater. Sci. Eng. A 430 (2006) 165–171.

[5] L. Anicai, A. Petica, S. Costovici, P. Prioteasa, T. Visan, Electrodeposition of Sn and NiSn alloys coatings using choline chloride based ionic liquids - evaluation of corrosion behavior, Electrochim. Acta 114 (2013) 868–877. Elsevier Ltd.

[6] C. Han, Q. Liu, D.G. Ivey, Nucleation of Sn and Sn-Cu alloys on Pt during electrodeposition from Sn-citrate and Sn-Cu-citrate solutions, Electrochim. Acta 54 (2009) 3419–3427.

[7] L. Mattarozzi, S. Cattarin, N. Comisso, P. Guerriero, M. Musiani, L. Vázquez-Gómez, E. Verlato, Electrochemical reduction of nitrate and nitrite in alkaline media at CuNi alloy electrodes, Electrochim. Acta 89 (2013) 488–496. Elsevier Ltd.

[8] P.Y. Chen, M.J. Deng, D.X. Zhuang, Electrochemical codeposition of copper and manganese from room-temperature N-butyl-N-methylpyrrolidinium bis(trifluoromethylsulfonyl)imide ionic liquid, Electrochim. Acta 54 (2009) 6935–6940.

[9] A. Brenner, Electrodeposition of Alloys: Principles and Practice, first ed., Academic press, New York), 1963.

[10] L.F. Senna, S.L. Diaz, L. Sathler, Electrodeposition of copper – zinc alloys in pyrophosphate-based electrolytes, J. Appl. Electrochem. 33 (2003) 1155–1161.

[11] F.B.A. Ferreira, F.L.G. Silva, A.S. Luna, D.C.B. Lago, L.F. Senna, Response surface modeling and optimization to study the influence of deposition parameters on the electrodeposition of Cu–Zn alloys in citrate medium, J. Appl. Electrochem. 37 (2007) 473–481.

[12] I.A. Carlos, M.R.H. De Almeida, Study of the influence of the polyalcohol sorbitol on the electrodeposition of copper-zinc films from a non-cyanide bath, J. Electroanal. Chem. 562 (2004) 153–159.

[13] F.H. Assaf, S.S. Abd El Rehim, A.S. Mohamed, A.M. Zaky, Electroplating of brass from citrate-based alloy baths, Indian J. Chem. Technol. 2 (3) (1995) 147–152.

[14] T.V., J.S.L.L, J.R. Moon, On the problems of topology, Electrochim. Acta 24 (1979) 231–236.

[15] Y. Fujiwara, H. Enomoto, Electrodeposition of B′-brass from cyanide baths with accumulative underpotential deposition of Zn, J. Electrochem. Soc. 147 (2000) 1840.

[16] A.Y. Musa, Q.J.M. Slaiman, A.A.H. Kadhum, M.S. Takriff, Effects of agitation, current density and cyanide concentration on Cu-Zn alloy electroplating, Eur. J. Sci. Res. 22 (2008) 517–524.

[17] K. Johannsen, D. Page, S. Roy, A systematic investigation of current efficiency during brass deposition from a pyrophosphate electrolyte using RDE, RCE, and QCM, Electrochim. Acta 45 (2000) 3691–3702.

[18] C. Ramírez, J.A. Calderón, Study of the effect of triethanolamine as a chelating agent in the simultaneous electrodeposition of copper and zinc from non-cyanide electrolytes, J. Electroanal. Chem. 765 (2016) 132–139. Elsevier B.V.

[19] M.R.H. de Almeida, E.P. Barbano, M.F. de Carvalho, I.A. Carlos, J.L.P. Siqueira, L.L. Barbosa, Electrodeposition of copper-zinc from an alkaline bath based on EDTA, Surf. Coating. Technol. 206 (2011) 95–102. Elsevier B.V.

[20] R.R. Povetkin, V.V. Zakharov, M.S. Muslimov, Electrodeposition of copper-zinc alloys from trilonate electrolytes, Russ. J. Appl. Chem. 72 (1999) 1367–1370.

[21] A.R. Despić, V. Marinović, V.D. Jović, Kinetics of deposition and dissolution of brass from the pyrophosphate-oxalate bath, J. Electroanal. Chem. 339 (1992) 473–488.

[22] R. Juškenas, V. Karpavičiene, V. Pakštas, A. Selskis, V. Kapočius, Electrochemical and XRD studies of Cu-Zn coatings electrodeposited in solution with D-mannitol, J. Electroanal. Chem. 602 (2007) 237–244.

[23] A. Survila, Z. Mockus, S. Kanapeckaite, G. Stalnionis, Kinetics of zinc and copper reduction in gluconate-sulfate solutions, Electrochim. Acta 94 (2013) 307–313.

[24] E. Guaus, J. Torrent-Burgués, Tin-zinc electrodeposition from sulphate-tartrate baths, J. Electroanal. Chem. 575 (2005) 301–309.

[25] E. Chassaing, K. Vu Quang, R. Wiart, Kinetics of copper electrodeposition in citrate electrolytes, J. Appl. Electrochem. 16 (1986) 591–604.

[26] A. Keyvani, M. Yeganeh, H. Rezaeyan, Electrodeposition of Zn-Co-Mo alloy on the steel substrate from citrate bath and its corrosion behavior in the chloride media, J. Mater. Eng. Perform. 26 (2017) 1958–1966. Springer US.

[27] D.-Y. Park, J.-M. Ko, Magnetic properties of nanocrystalline CoW thin film alloys electrodeposited from citrate baths, J. Korean Electrochem. Soc. 6 (2003) 236–241.

[28] T.P. Moffat, Material Research Society Symposium Proceeding, 1997, p. 451.

[29] D.M. Soares, S. Wasle, K.G. Weil, K. Doblhofer, Copper ion reduction catalyzed by chloride ions, J. Electroanal. Chem. 532 (2002) 353–358.

[30] G.G. Láng, M. Ujvári, G. Horányi, New EQCM, voltammetric and radiotracer evidences proving the role of Cu^{+} ions in the behavior of the Cu^{2+}-Cu system, J. Electroanal. Chem. 522 (2002) 179–188.

[31] W. Shao, G. Pattanaik, G. Zangari, Influence of chloride anions on the mechanism of copper electrodeposition from acidic sulfate electrolytes, J. Electrochem. Soc. 154 (2007) D201.

[32] J. Horkans, On the role of buffers and anions in NiFe electrodeposition, J. Electrochem. Soc. 126 (1979) 1861.

[33] E. Rudnik, Effect of anions on the electrodeposition of tin from acidic gluconate baths, Ionics (Kiel). 19 (2013) 1047–1059.

[34] J.C. Ballesteros, E. Chaînet, P. Ozil, G. Trejo, Y. Meas, Initial stages of the electrocrystallization of copper from non-cyanide alkaline bath containing Glycine, J. Electroanal. Chem. 645 (2010) 94–102. Elsevier B.V.

[35] J.C. Ballesteros, E. Chaînet, P. Ozil, G. Trejo, Y. Meas, Electrochemical studies of Zn underpotential/overpotential deposition on a nickel electrode from non-cyanide alkaline solution containing Glycine, Electrochim. Acta 56 (16) (2011) 5443–5451. Elsevier Ltd.

[36] K.-M. Yin, B.-T. Lin, Effects of boric acid on the electrodeposition of iron, nickel and iron-nickel, Surf. Coating. Technol. 78 (1–3) (1996) 205–210.

[37] C. Karwas, Morphology and composition of electrodeposited cobalt-zinc alloys and the influence of boric acid, J. Electrochem. Soc. 136 (1989) 1672.

[38] N. Zech, The influence of boric acid and sulfate ions on the hydrogen formation in Ni_Fe plating electrolytes, Electrochim. Acta 45 (2000) 3461–3471.

[39] L. Ricq, F. Lallemand, M.P. Gigandet, J. Pagetti, Influence of sodium saccharin on the electrodeposition and characterization of CoFe magnetic film, Surf. Coating. Technol. 138 (2001) 278–283.

[40] E. Chassaing, Effect of organic additives on the electrocrystallization and the magnetoresistance of Cu-Co multilayers, J. Electrochem. Soc. 148 (2001) C690–C694.

[41] L.H. Mendoza-Huizar, C.H. Rios-Reyes, M.G. Gômez-Villegas, Zinc electrodeposition from choloride solutions onto glassy carbón electrode, J. Mex. Chem. Soc. 53 (2009) 243–247.

[42] T. Jiang, M.J. Chollier Brym, G. Dubé, A. Lasia, G.M. Brisard, Electrodeposition of aluminium from ionic liquids: Part II - studies on the electrodeposition of aluminum from aluminum chloride (AlCl3) - trimethylphenylammonium chloride (TMPAC) ionic liquids, Surf. Coating. Technol. 201 (2006) 10–18.

[43] N.V.M. Daheum Kim, D.-Y. Park, B.Y. Yoo, P.T.A. Sumodjo, Magnetic properties of nanocrystalline CoW thin film alloys electrodeposited from citrate baths, J. Korean Electrochem. Soc. 6 (2003) 236–241.

[44] K.D.B.J.F. Moulder, W.F. Stickle, P.E. Sobol, Handbook of X-ray photoelectron spectroscopy, in: J. Chastain (Ed.), Pemkin-Elm, 1992. United State of America.

[45] S. M, P.A. Thiry, R. Caudano, J.J. Verbist, Interaction of O_2 with low index faces of α-CuZn, Surf. Sci. 127 (1983) 200–222.

[46] S. Chanel, N. Pébère, Investigation on the corrosion of brass-coated steel cords for tyres by electrochemical techniques, Corros. Sci. 43 (2001) 413–427.

[47] K. Yurdal, I.H. Karahan, A cyclic voltammetry study on electrodeposition of Cu-Zn alloy films: effect of ultrasonication time, Acta Phys. Pol., A 132 (2017) 1087–1090.

[48] Sunjung Kimz, David J. Duquette, Effect of chemical composition on adhesion of directly electrodeposited copper film on TiN, J. Electrochem. Soc. 153 (2006) C417–C421.

[49] M. Slupska, P. Ozga, Electrodeposition of Sn-Zn-Cu alloys from citrate solutions, Electrochim. Acta 141 (2014) 149–160. Elsevier Ltd.

[50] J. Lurie, in: Handbook Analytical Chemistry, M. Publishers, Moscou, 1978.

[51] L.T. de Farias, A.S. Luna, D.C.B. do Lago, L.F. de Senna, Influence of cathodic current density and mechanical stirring on the electrodeposition of Cu-Co alloys in citrate bath, Mater. Res. 11 (2008) 1–9.

[52] M. Pourbaix, in: Atlas of Electrochemical Equilibria in Aqueous Solutions, Pregamon P, Oxford), 1966.

[53] M. R, A.E.M. Smith, Critical Stability Constants, 1989. Plenum, Pr.